ACS OMEGA

http://pubs.acs.org/journal/acsodf

Article

Synergistic Effects of IMX-104 Components in Membrane Absorption: A Computational Study

Huarong Li,* Hong Yang, Mi Zhou, Tong Wei, and Yang Zhou*

Cite This: *ACS Omega* 2022, 7, 40892−40899

Read Online

ACCESS | Metrics & More | Article Recommendations | Supporting Information

ABSTRACT: New insensitive munitions such as IMX-104 formulations are being developed to improve the safety suffering from accidental stimulations. Experimental data indicated the synergistic toxicity of 2,4-dinitroanisole (DNAN) and hexahydro-1,3,5-trinitro-1,3,5-triazine (RDX) in IMX-104, which increased the concern about its environmental and health threats. Indeed, little is known about the synergistic mechanism. Here, we investigated the membrane absorption of DNAN and RDX as the first step toward uncovering synergistic toxicity. The permeability coefficient, transmembrane time, and liposome−water partition coefficient were calculated by the umbrella sampling technique. The results show that component RDX in the IMX-104 formulation promotes the membrane absorption of another more toxic component DNAN, suggesting that the synergistic toxicity effect of IMX-104 may emerge from their membrane adsorption stage. In detail, the integrating free-energy curves show that DNAN, RDX, or their mixture in membranes would promote subsequent molecules passing through membranes. For the mixture of DNAN and RDX, RDX was absorbed by the membrane before DNAN. Postabsorbed DNAN tends to stay around RDX, which is due to the strong van der Waals (VDW) interaction between them. RDX stabilized under phospholipid headgroups limits the overflow of DNAN from the membrane, which results in 11% more absorption of DNAN by the membrane than in the case of the pure DNAN system.

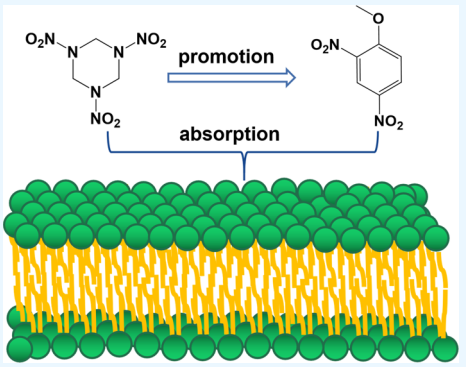

INTRODUCTION

Traditional explosives including 2,4,6-trinitrotoluene (TNT) and hexahydro-1,3,5-trinitro-1,3,5-triazine (RDX) are difficult to control the explosion risk of unintended stimulations during transport, manufacturing, and handling.[1] New insensitive munitions (IMs) are being developed to replace traditional high explosives to improve relative safety in terms of accidental explosions. Among them, the famous IMX-104 formulation, a mixture of 2,4-dinitroanisole (DNAN), 3-nitro-1,2,4-triazol-5-one (NTO), and RDX, has been qualified as a Composition B replacement.[2−5] However, recent toxicity studies suggested that components of IMX-104 have unique toxicological properties, which pose significant health and environmental threats. For example, NTO elicits toxicity by increased acidity at high concentrations in aquatic exposures.[6] The neurotoxic effects of RDX, such as seizures in humans, have been known for both humans and other mammals.[7] The aquatic toxicity of DNAN has been reported for cladocerans, tadpoles, and fish.[1,8] Especially, studies reported that the toxicity responses of DNAN-based IM mixtures were driven by the effective concentration of DNAN, which was much more toxic than other explosives, such as NTO and nitroguanidine (NQ).[9,10]

IM constituents are manufactured and discharged together, and the toxicity of chemical mixtures is very complex. Toxicity assessment of IM mixture formulations has lagged considerably relative to individual IM constituent evaluations.[8,10−12] Recently, Gust et al. reported that the acute toxic effects of IMX-104 mixture formulation exposed in fathead minnow larvae were 18% greater than the additive (or synergistic) effect.[13] DNAN and RDX, but not NTO, were characterized to contribute to the toxicity of IMX-104 by functional transcriptomics analysis. In addition, the transcriptomic responses to acute RDX and DNAN individual exposures showed that DNAN and RDX affected the transcriptional expression of Nrf2-associated kelch-like ECH-associated protein 1 (keap1), with some degree of confliction.[12,13] Finally, the potential mechanisms of synergistic toxicity within the IMX-104 mixture were hypothesized to be related to the interactive effects of each DNAN and RDX molecule. Toxicological interactions between organic compounds leading to synergistic toxic effects have been observed years ago.[14−16] Atrazine and terbuthylazine mixtures elicited synergistic responses on the swimming behavior of zebrafish larvae.[15] When investigating the synergistic interactions between the herbicide atrazine and the organophosphate insecticide chlorpyriphos to larvae of the midge Chironomus tentans, Belden and Lydy found that the addition of atrazine

Received: June 21, 2022
Accepted: October 19, 2022
Published: November 3, 2022

increased chlorpyriphos uptake by 40%.[16] Additive toxicity as slightly greater-than additive effects for a mixture of TNT, RDX, and 1,3,5,7-octahydro-1,3,5,7-tetranitrotetrazocine (HMX) was also observed in the earthworm *Eisenia fetita* exposed to spiked soils.[17] Nevertheless, thorough insights into the synergistic toxicity interaction mechanisms between the mixture molecules are still absent.

To target a cytosol (e.g., keap1), a drug molecule must be able to absorb in the lipid membrane,[18,19] which is of vital importance to study the progress of adsorption, distribution, metabolism, and excretion (ADME) in organisms. For example, the toxicity of canthaxanthin (*β*,*β*-carotene-4,4′-dione) to humans was strongly related to its transmembrane and interactions with the lipid membranes.[20] *α*-Synuclein eliciting Parkinson's disease might be the consequence of its abnormal interactions with the membrane.[21] Our previous work found that the monoamino metabolites of TNT had higher transmembrane capacity than their parent compound, which helps to explain why they are even more toxic than TNT.[22] It is still a challenge for experimental techniques to obtain a detailed molecular-level understanding of chemical−membrane interactions, and molecular simulation technology has been proved to be a useful tool for obtaining information about the penetration and distribution of small molecules in cell membranes and how they affect the properties of lipid bilayer membranes.[20,22,23] In the present work, we used the all-atom molecular dynamics (MD) method and umbrella sampling (US) technology to study the permeation process of RDX and DNAN mixtures, according to their molar ratio within IMX-104 formulation, from the water phase to the 1-palmitoyl-2-oleoyl-*sn*-glycerol-3-phosphocholine (POPC) phospholipid bilayer membrane, and investigate the effect of intermolecular interaction between RDX and DNAN on their entering into the membrane.

METHODS

Lipid Bilayer Model and Simulation Details. The lipid bilayer model consisting of 128 POPC lipids (with 64 in each leaflet) was constructed by CHARMM-GUI.[24] The bilayer was oriented perpendicular to the *z*-axis and surrounded by at least 12 500 water molecules. NaCl (0.15 M) was added to the system to maintain physiological concentration. The system was equilibrated for 100 ns, and the final simulation box for the pure membrane system (M-system) was about 6.5 × 6.5 × 13.0 nm^3.

First, we studied the dynamic behavior of 23 DNAN, 23 RDX, and DNAN/RDX mixtures containing 16 DNAN and 7 RDX in water. The results show that explosives in the three systems gathered into a large cluster in 3, 1, and 2 ns, respectively (Figure S1). The large clusters kept the aggregation state to the final simulation time (Figure S1), indicating that DNAN, RDX, or DNAN/RDX mixtures would aggregate together before reaching the membrane−water interface. Therefore, we chose a structure of aggregation state from their dynamic trajectories to insert in the *z*-direction in the range from 4.0 to 4.4 nm of the M-system and built another three simulation systems containing 23 DNAN (D-system), 23 RDX (R-system), and 7 RDX/16 DNAN (DR-system). The molar ratio of DNAN and RDX in the DR-system is the same as that in the IMX-104 formulation (DNAN/RDX = 16:7).[25]

All MD simulations were carried out with GROMACS 5.1.2 packages.[26] The all-atom CHARMM36 force field[27] was utilized to describe POPC lipids. Water molecules were described by the TIP3P model.[28] Newton's equations were integrated by the leapfrog algorithm with the time step of 2 fs. To constrain the bonds involving hydrogen atoms, the LINCS algorithm was chosen.[29] Bond lengths and angles of water were constrained by the SETTLE algorithm.[30] The particle mesh Ewald (PME) algorithm[31] was used to compute the electrostatic interaction with the real space cutoff of 1.2 nm, a grid spacing of 0.16 nm, and fourth-order interpolation. The van der Waals (VDW) interaction was switched smoothly to zero over the region between 1.0 and 1.2 nm. Periodic boundary conditions were used in all directions. To maintain the pressure at about 1 bar, all of the simulations were performed at 310 K in the NPT ensemble using the velocity-rescaling thermostat[32] with a time constant of 0.2 ps. The semi-isotropic Parrinello−Rahman algorithm[33] chose a time constant of 1 ps and a compressibility of 4.5 × 10^{-5} bar^{-1}. Energy minimizations were performed by the steepest descent algorithm.

Additionally, the parameters of DNAN were derived from CHARMM General Force Field (CGenFF)[34] and had been successfully used in our previous work.[23] In particular, because of its nonplanar N-heterocyclic and N-NO_2 functional groups, almost all of the parameters of RDX are not included in the standard CGenFF (Figure 1). Herein, we calculated the force

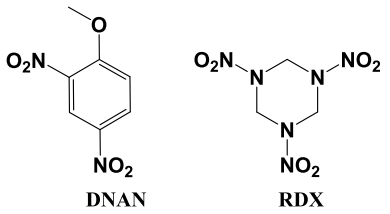

Figure 1. Molecular structures of DNAN and RDX.

field parameters of RDX (RDX.itp and RDX.prm in the Supporting Information) by the ffTK program.[35] To validate the force field parameters, we calculated the 1-octanol−water partition coefficient (log K_{OW}) of RDX by the free energy perturbation method (eqs S1 and S2). The calculated log K_{OW} (1.42) and experimental log K_{OW} (0.87)[36] show a 1:1 agreement with differences of 0.55 log unit. The area per lipid is also used as a check for force field parameters in MD studies and characterizing the change in the overall architecture of the bilayer after the permeation of drugs.[37] We calculated the area per lipid of the DR-system using a statistical average area of the simulation box that is perpendicular to the membrane normal (defined by the *x*- and *y*-size of the box, Supporting Information named *x*- and *y*-size of the box with simulation time.txt) divided by the number of lipids per leaflet (64). Our calculated area per lipid is 42.153 nm^2/64 = 0.659 nm^2 (310 K), which is almost the same as the experimental value of 0.658 nm^2 (271 K).[38]

Potential of Mean Force (PMF) Calculations. The free energy (Δ*G*) profiles (or potentials of mean force, PMFs) of the two explosives across the lipid bilayer model were obtained by umbrella sampling. The initial structures of a series of 32 separate windows were prepared by pulling the solute molecules along the *z*-direction from the water phase (*z* = 4 nm) to the center of the bilayer (*z* = 0 nm), with the spacings of 0.2 nm in the water phase and 0.1 nm inside the membrane. During each MD simulation, an umbrella restraint was only applied to the solute molecules along the z-direction, and the solutes can move freely in the *x*−*y* plane. The force constant of the harmonic spring was 1000 kJ mol^{-1} nm^{-2} for all windows, ensuring the

https://doi.org/10.1021/acsomega.2c03886
ACS Omega 2022, 7, 40892−40899

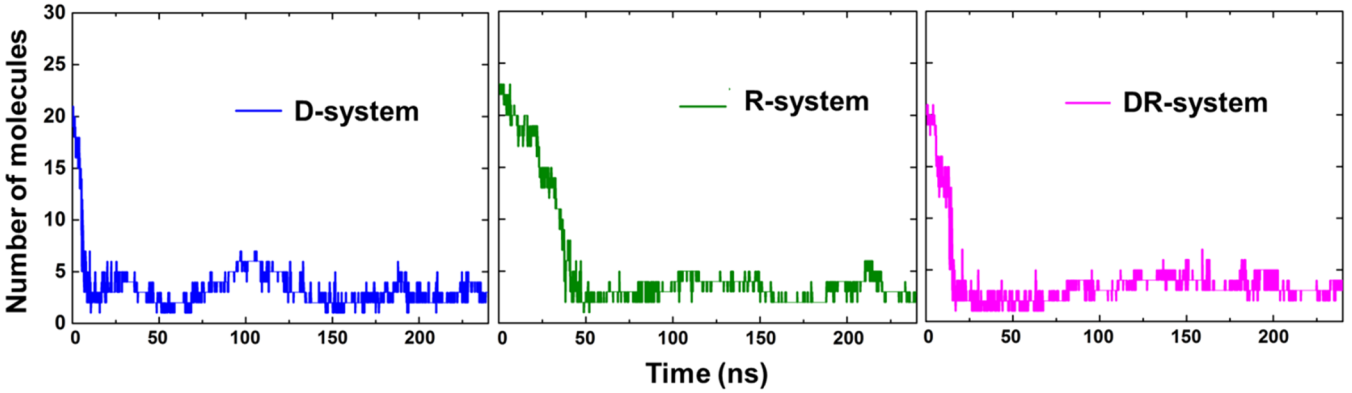

Figure 2. Number of explosives contained in the largest aggregates with the simulation time for D-system, R-system, and DR-system.

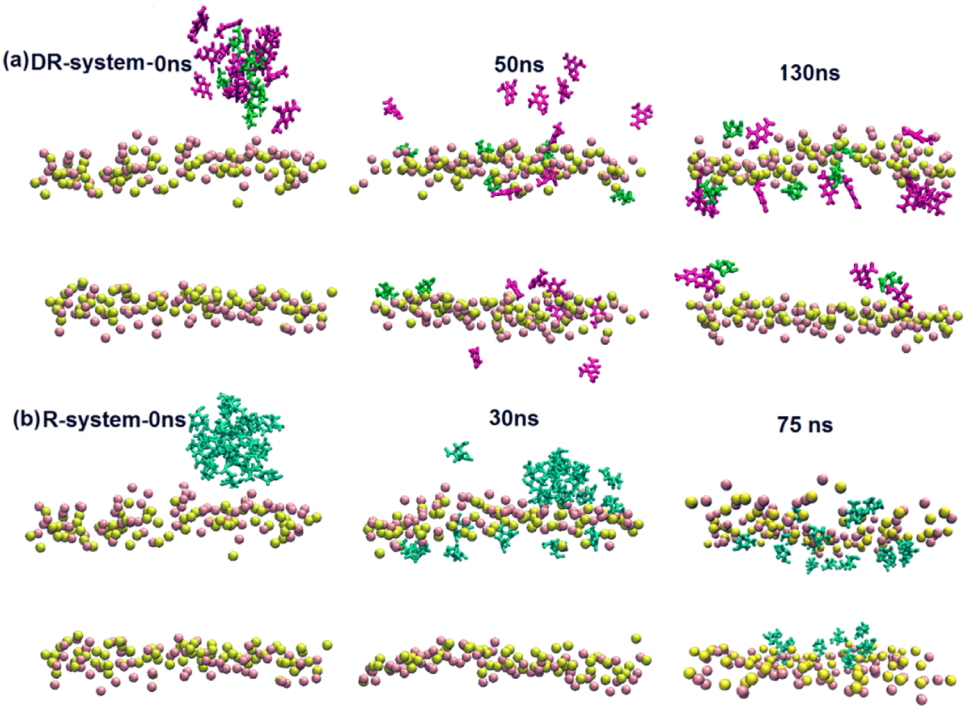

Figure 3. Snapshots depicting the partition process of DNAN and RDX molecules into (a) DR-system and (b) R-system. P and N on POPC are displayed in pink and yellow. RDX and DNAN are in green and purple, respectively. Water and ions are not shown for clarity.

adequate sampling of the simulations. Each window was run for 50 ns and the last 20 ns of trajectories were used for the calculation of PMF profiles.[23] Due to membrane symmetry, we only calculated the free energy profiles from z = 4 nm to z = 0 nm. The free energy profiles were computed by the weighted histogram analysis method (WHAM).[39] The Bayesian bootstrap analysis (N = 100) was utilized to obtain an estimation of the statistical error for PMF profiles.[40]

Three Key Parameters for Describing the Behavior of Permeation and Partitioning. Three key parameters for describing the behavior of permeation and partitioning, namely, liposome−water partition coefficient (K_{LW}), permeability coefficient (P), and translocation time (τ), can be obtained by free energy landscapes.

K_{LW} is defined as the ratio of the concentration of the compound when the lipid phase and the water phase reach an equilibrium. It was calculated according to the free energy profiles as presented in eq 1[41]

$$K_{LW} = \frac{\sum_{i=1}^{n}\left[V(z_i)\exp(-\beta\Delta G(z_i)) - V(z_n)\exp(-\beta\Delta G(z_n))\frac{x_w(z_i)}{x_w(z_n)}\right]}{V(z_n)\exp(-\beta\Delta G(z_n))\frac{1}{x_w(z_n)}} \times \frac{V_W}{V_L} \quad (1)$$

where the system is split into n layers along the z-direction, and layer n belongs to the water phase. $\Delta G(z_i)$ is the free energy at z_i; $\beta = 1/k_B$, where k_B is the Boltzmann constant; $x_w(z_i) = n_w(z_i)/n_w^{tot}$, where $n_w(z_i)$ and n_w^{tot} are the number of water molecules in layer i and in the system, respectively; and v_L and v_W are the volumes of the lipid phase and the water phase, respectively.

P describes the speed of molecules across the cell membrane. P can be estimated according to the inhomogeneous solubility diffusion model,[42] in which P is expressed as a function of $\Delta G(z)$ and diffusion coefficient $D(z)$, as shown in the following equations

$$P = \left[\int_{-4\text{ nm}}^{4\text{ nm}} \frac{e^{\Delta G(z)/RT}}{D(z)} dz\right]^{-1} \quad (2)$$

https://doi.org/10.1021/acsomega.2c03886
ACS Omega 2022, 7, 40892−40899

$$D(z) = \frac{(RT)^2}{\int_0^\infty \langle \Delta F(z, t) \Delta F(z, 0) \rangle \mathrm{d}t} \quad (3)$$

$$\Delta F(z, t) = F(z, t) - \langle F(z, t) \rangle \quad (4)$$

where R is the gas constant, T is the temperature (K), and $F(z,t)$ is the constrained force on the solute at a given z-position along the normal direction.

τ estimates the time for solutes to cross the membrane from one side of the lipid bilayer to the other. By the assumption of Brownian motion, τ can be obtained from eq 5[43]

$$\tau = \frac{1}{D_z} \int_{-4\ \mathrm{nm}}^{4\ \mathrm{nm}} e^{\Delta G(y)/RT} \mathrm{d}y \int_{-4\ \mathrm{nm}}^{y} e^{-\Delta G(z)/RT} \mathrm{d}z \quad (5)$$

where D_z is the diffusion coefficient of solutes in the transmembrane direction (z-direction). In the order of magnitude estimate of the translocation time, we are not interested in the changes of D_z with depth. Therefore, we used D_z at free-energy minimum in this calculation, as the solutes mostly reside in this region.

RESULTS AND DISCUSSION

Membrane Adsorption of Molecules. At first, we investigated the process of 23 DNAN, 23 RDX, and DNAN/RDX mixture containing 16 DNAN and 7 RDX entering the lipid bilayer from the aqueous phase at the same concentration (17 mol %). Initially, the explosives arrived at the membrane−water interfaces in aggregation states (Figure S1), corresponding to 0 ns of the three systems (Figure 2). To quantitatively describe the aggregate (or cluster), we characterized the aggregate size by counting the number of explosive molecules in the largest aggregate. As seen in Figure 2, the clusters scattered gradually and became individual molecules or smaller clusters (two to three molecules). The breaking-up time for the large aggregate of DNAN, RDX, and DNAN/RDX mixtures were 8.5, 47, and 16.5 ns, respectively. The significant difference in the aggregate breaking time suggests that the processes of membrane adsorption for the three systems might be different. From the snapshots depicting the partition process of DNAN and RDX molecules into lipid membranes (Figure 3), we can find that RDX would preferentially penetrate into the membrane over the DNAN molecules. All RDX molecules in the DR-system reside in the membrane at 50 ns (Figure 3a), and the RDX molecules are far from each other. At 130 ns, all DNAN molecules in the DR-system are observed to move to the inside of the membrane. The penetrated RDX and DNAN molecules dispersed in the head region of the POPC membrane in form of dimers, trimers, and tetramers with the simulation time.

To further explore the membrane absorption process, we calculated the average molar percentage (M) of DNAN and RDX in the membrane by the molar density profiles along the bilayer normal (z-direction) in different systems (Figure S3 and Table 1), according to the following equation

$$M = \frac{n\_\mathrm{DNANs-DR}}{n\_\mathrm{total}} \times 100\% \quad (6)$$

where n_DNANs-DR is the average molar number of DNAN in the lipid bilayer ($-2\ \mathrm{nm} < z < 2\ \mathrm{nm}$) and n_total (n_total = n_DNANs-DR + n_DNAN in water) is the molar number of total explosives in the considered systems. The value of n_total is identical in the present three systems (about 3590 mol/m^3) because the molar ratio for explosives in the three systems is 17 mol %.

Table 1. Molar Percentages of DNAN and RDX in the Lipid Bilayers

	M (%)				
compound[a]	the first 30 ns	30−60 ns	150−180 ns	180−210 ns	the last 30 ns
RDXs-DR	56	61	77	85	85
RDXs-R	25	48	81	85	86
DNANs-DR	19	37	78	76	78
DNANs-D	42	46	60	66	67

[a]RDXs-DR denotes the RDX molecules in the lipid bilayer of the DNAN and RDX mixture system. RDXs-R denotes the RDX molecules in the lipid bilayer of the R-system. DNANs-DR denotes DNAN in the bilayer of the DNAN and RDX mixture system. DNANs-D denotes DNAN in the bilayer of the D-system.

In the first 30 ns, RDX was found to preferentially penetrate into the membrane over DNAN molecules. In detail, the M of RDXs-DR and DNANs-DR are 56 and 19%, respectively. It is worth noting that there is still a stable aggregate of about 13−15 RDX molecules in the RDX-system at 30 ns (Figure 3b). The M of RDXs-R is only 25%. It reveals that the stable aggregation might reduce the speed of RDX molecules entering the cell membrane. From the next 30 ns (30−60 ns), DNANs-DR was adsorbed rapidly, and the number of RDXs-DR increased lesser. During the simulation time of the last 90 ns (150−180, 180−210, and 210−240 ns), the molar percentage of DNAN and RDX in all of the membranes changed little, indicating that the small molecules in the lipid phase and the water phase reached an equilibrium. In the last 30 ns (210−240 ns), the molar percentage of more toxic DNAN in the lipid bilayer increased from 67% (DNANs-D) to 78% (DNANs-DR), indicating an increase of membrane adsorption for a more toxic DNAN. We can also find that the molar percentages of RDXs-DR (86%) and RDXs-R (85%) are both more than those of DNANs-DR and DNANs-R. In the next part, we used US technology to further explore the mixture effect on the membrane adsorption of DNAN and RDX.

Single-Molecule Simulations. *PMF Profiles.* The PMF profiles of DNAN and RDX crossing four different lipid bilayers were plotted (Figure 4 and Table 2). The value of the free energy at z = 4 nm (i.e., in the aqueous phase) is set to zero. As can be seen from Figure 4, the free energy sharply drops to a minimum after the membrane entry (ΔG_D), meaning that each DNAN and RDX can spontaneously enter into the membrane interior from bulk water in all of the considered systems. The ΔG_D of RDX (−11.7 kJ/mol) in a pure system (RDX-M) is almost equal to that of 2,4,6-triamino-1,3,5-trinitrobenzene (TATB, −12.1 kJ/mol).[23] We judge that the membrane partitioning of RDX is mainly driven by the nitrogen heterocyclic ring, and the effect is equivalent to that of the benzene ring. As seen in Table 2, the ΔG_D of RDX in the four systems is larger than that of DNAN, indicating that it is easier for RDX to enter the membranes than for DNAN. The value of the energy barriers (ΔG_B), which can be defined as the difference between the free-energy maximum (ΔG_max) and minima (ΔG_min), shows that ΔG_B of RDX is larger than that of DNAN in the four systems, indicating that RDX is more likely to stay in the membrane. Compared with the barrier of RDX-R (20.1 kJ/mol) across the membrane, the barrier of RDX-DR (21.2 kJ/mol) and RDX-D (24.1 kJ/mol) increases by 5 and 12%, respectively. More DNAN molecules in the

https://doi.org/10.1021/acsomega.2c03886
ACS Omega 2022, 7, 40892−40899

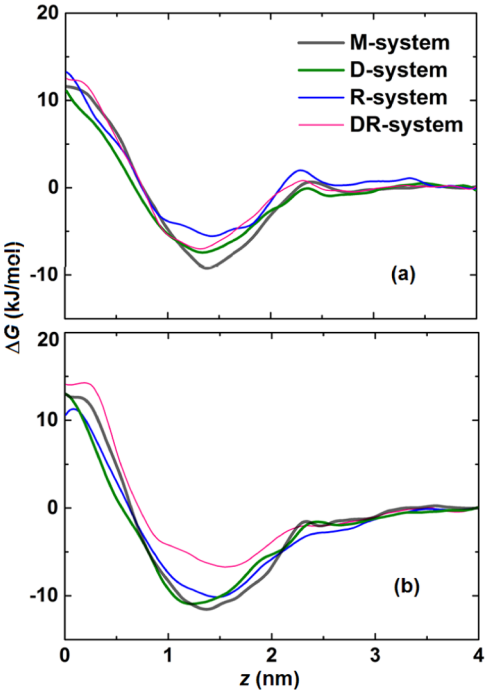

Figure 4. PMF profiles along the normal of the membrane (z-direction) as a function of the distance from the bilayer center (z = 0) for (a) a DNAN molecule and (b) an RDX molecule in four membrane systems.

membrane were expected to inhibit RDX crossing the membrane. The energy barriers of DNAN-D (18.5 kJ/mol) and DNAN-R (18.6 kJ/mol) are almost the same, and the barrier increases by 5% for DNAN-DR (19.7 kJ/mol). Also, the increase of the energy barriers for these two molecules might be caused by the intermolecular interaction between DNAN and RDX.

The preferred location (z_{min}) of DNAN and RDX is in the range from 1.25 to 1.61 nm, indicating that they prefer to locate in the headgroup region (1.3 nm < z_{min} < 2 nm) (Figure S2).[42,44] As shown in Figure 4 and Table 2, DNAN-M and RDX-M possess the same z_{min} (1.39 nm). The z_{min} of DNAN-D (1.37 nm) and RDX-D (1.25 nm) tend to the back of the head region of the membrane. On the other hand, the z_{min} of DNAN-R (1.45 nm) and RDX-R (1.47 nm) move slightly toward the head region of the membrane. However, RDX-DR (z_{min} = 1.61 nm) is closer to the head region of the membrane, and DNAN-DR is slightly closer to the hydrophobic center of the lipid bilayer (z_{min} = 1.31 nm). From the density profiles in the DR-system (Figure S3d), we found that RDX molecules entering the membrane in the last 30 ns of simulations have the density peak at $z = \pm(1.6-1.7)$ nm, and most DNAN molecules prefer to locate at $z = \pm 1.3$ nm, corresponding well to z_{min} on PMF profiles (Figure 4).

Key Parameters. To quantitatively describe the mixture effect of DNAN and RDX on their membrane adsorption, we calculate the three key parameters that describe the behavior of membrane permeation and partitioning, namely, K_{LW}, P, and τ. K_{LW} was suggested to be a more accurate descriptor than the common K_{OW}. We calculated log K_{LW} of DNAN and RDX according to eq 1, and the results are listed in Table 2. It can be seen that the log K_{LW} for DNAN and RDX in a pure membrane are 1.02 and 1.46, indicating that these two explosives have the ability to cross the lipid membrane. Zeliger et al. reported that a lipophilic species promotes the permeation of a hydrophilic species through a mucous membrane in all exposures to mixtures of chemicals with varying partition coefficient values.[45] It appears that DNAN belongs to a class of relative hydrophilic chemicals, and RDX belongs to a class of relative hydrophobic chemicals.[46] The presence of RDX might promote the membrane adsorption of DNAN.

Our previous work suggested that P was greatly influenced by the functional group, especially polar groups (−OH, $-NO_2$, $-NH_2$, $-OCH_3$).[22,23] As DNAN and RDX both contain three polar groups, it is not surprising that the value of P for these two molecules in different systems is almost identical (Table 2). It also indicates that the membrane structures are not damaged, which is proved by the evolution of the density profiles along the bilayer normal (z-direction) for lipids and water in the DR-system (Figure S2). Then, we calculated the translocation time (τ) of DNAN and RDX to pass through a phospholipid membrane in the four systems. As listed in Table 2, the τ of DNAN and RDX molecules in the present systems is several μs; therefore, it is difficult to observe a complete transmembrane event in the unconstrained simulations with only hundreds of ns. The τ of DNAN and RDX crossing the other three membranes is slightly shorter than that of the pure membrane. We deduce that DNAN and RDX or their mixture previously entering the membrane will slightly promote subsequent DNAN and RDX crossing through the membrane, which agrees with the result that the energy barrier (ΔG_B) of DNAN (or RDX) in the pure system is larger than in the three other systems. Furthermore, both DNAN and RDX in the DR-system need slightly more time to pass through the bilayer than in the D-system and the R-system, implying the mixture effect of DNAN and RDX.

Role of Hydrogen Bonds (H-Bonds) and Intermolecular Interaction. *H-Bonds.* The processes of solutes leaving the aqueous phase and entering the membrane are accompanied by the destruction of the H-bonds network and the loss of H-bonds.

Table 2. Calculated Transport Properties of DNAN and RDX in Different Systems

compound[a]	ΔG_D(kJ/mol)	ΔG_B(kJ/mol)	ΔG_{max}(kJ/mol)	P(cm/s)	z_{min} (nm)	log K_{LW}	τ (μs)
DNAN-M	−9.3	20.9	11.6	0.32	1.39	1.02	6.85
DNAN-D	−7.5	18.5	11.0	0.60	1.35		2.37
DNAN-R	−5.7	18.6	12.9	0.45	1.45		2.63
DNAN-DR	−7.1	19.7	12.6	0.67	1.31		3.69
RDX-M	−11.7	24.5	12.8	0.19	1.39	1.46	32.4
RDX-D	−11.1	24.1	13.0	0.38	1.25		11.04
RDX-R	−8.6	20.1	11.5	0.71	1.47		4.61
RDX-DR	−6.8	21.2	14.4	0.11	1.61		11.89

[a]DNAN-M, DNAN-D, DNAN-R, and DNAN-DR denote DNAN in M-system, D-system, R-system, and DR-system, respectively. RDX-M, RDX-D, RDX-R, and RDX-DR denote RDX in M-system, D-system, R-system, and DR-system, respectively.

https://doi.org/10.1021/acsomega.2c03886
ACS Omega 2022, 7, 40892−40899

The hydrogen-bonding ability of solutes plays a critical role during their transport across biomembranes.[47,48] We calculated the number of H-bonds of DNAN and RDX molecules with water molecules from the water phase (z = 4 nm) to the center of the bilayer (z = 0 nm) in the four systems. The definition of hydrogen bond was the default criterion of the GROMACS package. It is obvious that the number of H-bonds of RDX-DR remains about 1 from entering the head region of the membrane to near the center of the membrane, and there must be a water molecule around RDX during its partition, which can be proved by the snapshot at the right bottom of Figure 5b. In addition, we

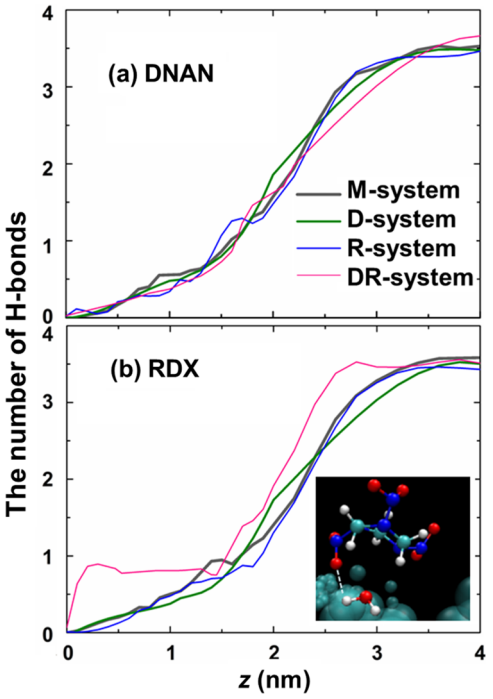

Figure 5. H-bonds between solute molecules and the surrounding water molecules from the water phase (z = 4 nm) to the center of the bilayer (z = 0 nm) for (a) DNAN and (b) RDX in different membranes.

found that the H-bonds in the preferred location can affect the location of solutes inside the membrane (Table 3). The number

Table 3. H-Bonds of DNAN and RDX at z_{min}

compound	NO_2-SOL	OCH_3-SOL	total
DNAN-M	0.6	0.2	0.8
DNAN-D	0.4	0.2	0.7
DNAN-R	0.7	0.2	0.9
DNAN-DR	0.3	0.2	0.5
RDX-M	0.9		0.9
RDX-D	0.5		0.5
RDX-R	0.7		0.7
RDX-DR	1.1		1.1

of hydrogen bonds for both DNAN-M and RDX-M at z_{min} is 0.7 and that in water (z = 4 nm) is 3.5 and 3.6, respectively. Also, DNAN-M and RDX-M locate at the same z_{min} (1.39 nm). It can be found that the $-NO_2$ group and $-OCH_3$ group have the same effect on the ability of these two explosives to form H-bonds with water molecules. In all, the higher the number H-bonds at the preferred location, the closer the preferred region of solutes is to the head groups of the membrane. However, the number of H-bonds for these two explosives in all of the systems decreases to less than 1 from z_{min} to the center of the lipid bilayer (nearly zero), meaning that the H-bonds in the membrane are not strong enough to control the ability of DNAN and RDX to pass through the membrane.

VDW Interactions. Our previous work suggested that TNT molecules previously entering the membrane will promote the permeability of the latter molecules in the membrane, and the VDW interactions between TNT molecules play the main role in their attraction and clustering.[22] Wang et al. reported that 8 mol % of cimetidine would lead to a decrease in the ability of subsequent cimetidine molecules across the membrane, which was attributed to the insignificant interactions between cimetidine molecules.[49] Therefore, we calculated the VDW energy between the explosive molecules during their membrane adsorption process in a mixture system. It can be seen from Figure 6 that the VDW energy between RDX molecules (VMD-

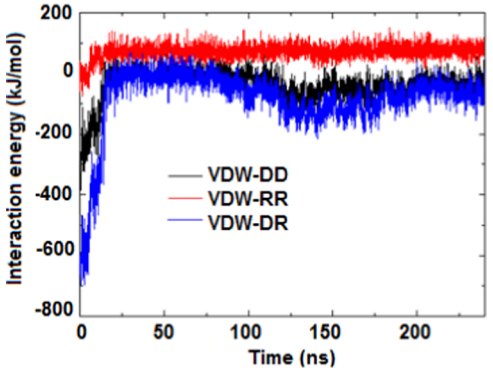

Figure 6. VDW energy of DNAN and RDX molecules with the simulation time for 16 DNAN/7 RDX entering POPC membrane from the aqueous phase.

RR) is very weak and quickly decreased to almost zero, even showing repulsion to each other. The value of VDW energy between DNAN and RDX (VDW-DR) and DNAN molecules (VDW-DD) decreases gradually from several hundred to zero from 0 ns to about 15 ns and is maintained at about zero during the next 50 ns, indicating that RDX/DNAN clusters break up and become individual molecules to enter the membrane. At about 130 ns, when most DNAN had been in the lipid bilayer, VDW-DR gradually increased again, implying the formation of DNAN and RDX dimers or multimers in the lipid bilayer. Therefore, we conclude that RDX tends to aggregate with DNAN rather than with itself in the lipid bilayer, and these results prove our observing snapshots in Figure 3a. Accordingly, the value of VDW-DR is stronger than that of VDW-DD and VDW-RR, which may contribute to the promotion of membrane adsorption for DNAN.

CONCLUSIONS

In summary, the membrane adsorption of 16 DNAN (12 mol %) and 7 RDX (7 mol %) mixtures revealed a synergistic absorption effect for more toxic DNAN molecules, that is, the molar percentage of DNANs-DR (78%) is 11% more than that of DNANs-D (67%). Also, the molar percentage of RDXs-DR (85%) and RDXs-R (86%) are nearly identical. It can be inferred that the molar percentage of membrane absorption increase for the DNAN molecules is due to the presence of RDX molecules. The PMF curves show that these two kinds of molecules enter the four systems (M-system, D-system, R-system, DR-system)

https://doi.org/10.1021/acsomega.2c03886
ACS Omega 2022, 7, 40892−40899

spontaneously. The value of P and τ reveal that DNAN and RDX or their mixture previously entering the lipid bilayer will slightly promote subsequent DNAN and RDX penetrating through the lipid bilayer and entering cells. The energy barrier for RDX across the membrane is higher than that of DNAN, indicating that RDX is more likely to stay in the lipid membrane than DNAN. DNAN in the membrane was expected to inhibit RDX crossing the membrane, and the energy barrier of RDX increased with the concentration of DNAN. The H-bonds in all of the considered systems are not strong enough to control the ability of DNAN and RDX to pass through the membrane. Based on the unconstrained MD simulations and the intermolecular interaction energy analyzing (VDW-DR, VDW-DD, and VDW-RR), it can be concluded that RDX in the mixture system will preferentially penetrate into the membrane over DNAN. RDX molecules disperse in the head of the lipid membrane and catch the DNAN molecules entering, subsequently preventing them from returning to the water again by forming dimers or multimers with them. Therefore, we infer that the synergistic toxicity effect may emerge from the membrane entry process, and VDW interactions played a critical role in this process.

Clearly, the results in this work are only a first step toward a better understanding of mixture toxicology for IMX-104 components. In our next work, we will focus on the interaction between explosive molecules and their targeted protein keap1,[12,13] which is a key expression-related protein in toxicity tests for many drug molecules in addition to DNAN and RDX.[50]

■ ASSOCIATED CONTENT

Supporting Information

The Supporting Information is available free of charge at https://pubs.acs.org/doi/10.1021/acsomega.2c03886.

Calculation equations of log K_{OW} for RDX; the number of explosives contained in the largest aggregate with the simulation time for explosive molecules in water; the evolution of the density profiles along the bilayer normal (z-direction) for lipids and water in DR-system; and the evolution of the density profiles along the bilayer normal (z-direction) for DNAN and RDX in different systems (PDF)

Force field parameters of RDX (RDX.itp and RDX.prm) (TXT)

■ AUTHOR INFORMATION

Corresponding Authors

Huarong Li − *Institute of Chemical Materials, China Academy of Engineering and Physics, Mianyang 621900, China;* orcid.org/0000-0001-7080-6462; Email: 215699921@qq.com

Yang Zhou − *Institute of Chemical Materials, China Academy of Engineering and Physics, Mianyang 621900, China;* orcid.org/0000-0003-3055-6491; Email: zhouy@caep.cn

Authors

Hong Yang − *Institute of Chemical Materials, China Academy of Engineering and Physics, Mianyang 621900, China*

Mi Zhou − *Institute of Chemical Materials, China Academy of Engineering and Physics, Mianyang 621900, China*

Tong Wei − *Institute of Chemical Materials, China Academy of Engineering and Physics, Mianyang 621900, China*

Complete contact information is available at: https://pubs.acs.org/10.1021/acsomega.2c03886

Notes

The authors declare no competing financial interest.

■ ACKNOWLEDGMENTS

All the authors appreciate very much the financial support from the National Natural Sciences Foundation of China (No. 21905260).

■ REFERENCES

(1) Stanley, J. K.; Lotufo, G. R.; Biedenbach, J. M.; Chappell, P.; Gust, K. A. Toxicity of the Conventional Energetics TNT and RDX Relative to New Insensitive Munitions Constituents DNAN and NTO in *Rana pipiens* Tadpoles. *Environ. Toxicol. Chem.* **2015**, *34*, 873−879.

(2) Singh, S.; Jelinek, L.; Samuels, P.; Di Stasio, A.; Zunino, L. In *IMX-104 Characterization for DoD Qualification*, 2010 Insensitive Munitions & Energetic Materials Technology Symposium, Munich, October 2010.

(3) Provatas, A.; Wall, C. In *Thermal Testing of 2,4-dinitroanisole (DNAN) as a TNT Replacement for Melt Cast Explosive*, 42th International Annual Conference of ICT, Karlsruhe, 2011.

(4) Oxley, J. C.; Smith, J. L.; Donnelly, M. A.; Colizza, K.; Rayome, S. Thermal Stability Studies Comparing IMX-101 (Dinitroanisole/Nitroguanidine/NTO) to Analogous Formulations Containing Dinitrotoluene. *Propellants Explos. Pyrotech.* **2016**, *41*, 98−113.

(5) Trzciński, W.; Cudziło, S.; Dyjak, S.; Nita, M. A Comparison of the Sensitivity and Performance Characteristics of Melt-pour Explosives with TNT and DNAN Binder. *Cent. Eur. J. Energ. Mater.* **2014**, *11*, 443−455.

(6) Pillard, D. A.; Eck, W. S.; Johnson, M. S.; Packard, S. Effects of 3-Nitro-1,2,4-triazol-5-one on Survival, Growth and Metamorphosis in the Northern Leopard Frog, Lithobates Pipien. *Ecotoxicology* **2017**, *26*, 1170−1180.

(7) Bannon, D. I.; Williams, L. R.*Wildlife Toxicity Assessment for 1,3,5-Trinitrohexahydro-1,3,5-triazine (RDX)*; Elsevier, 2015; pp 53−86.

(8) Kennedy, A. J.; Poda, A. R.; Melby, N. L.; Moores, L. C.; Jordan, S. M.; Gust, K. A.; Bednar, A. J. Aquatic Toxicity of Photo-degraded Insensitive Munition 101 (IMX-101) Constituents. *Environ. Toxicol. Chem.* **2017**, *36*, 2050−2057.

(9) Lotufo, G. R.; Stanley, J. K.; Chappell, P.; Melby, N. L.; Wilbanks, M. S.; Gust, K. A. Subchronic, Chronic, Lethal and Sublethal Toxicity of Insensitive Munitions Mixture Formulations Relative to Individual Constituents in *Hyalella azteca*. *Chemosphere* **2018**, *210*, 795−804.

(10) Temple, T.; Ladyman, M.; Mai, N.; Galante, E.; Ricamora, M.; Shirazi, R.; Coulon, F. Investigation into the Environmental Fate of the Combined Insensitive High Explosive Constituents 2,4-Dinitroanisole (DNAN), 1-Nitroguanidine (NQ) and Nitrotriazolone (NTO) in Soil. *Sci. Total Environ.* **2018**, *625*, 1264−1271.

(11) Fuller, M. E.; Rezes, R. T.; Hedman, P. C.; Jones, J. C.; Sturchio, N. C.; Hatzinger, P. B. Biotransformation of the Insensitive Munition Constituents 3-Nitro-1,2,4-triazol-5-One (NTO) And 2, 4-Dinitroanisole (DNAN) by Aerobic Methane-Oxidizing Consortia and Pure Cultures. *J. Hazard. Mater.* **2021**, *407*, No. 124341.

(12) Warner, C. M.; Gust, K. A.; Stanley, J. K.; Habib, T.; Wilbanks, M. S.; Garcia-Reyero, N.; Perkins, E. J. A Systems Toxicology Approach to Elucidate the Mechanisms Involved in RDX Species-Specific Sensitivity. *Environ. Sci. Technol.* **2012**, *46*, 7790−7798.

(13) Gust, K. A.; Lotufo, G. R.; Stanley, J. K.; Wilbanks, M. S.; Chappell, P.; Barker, N. D. Transcriptomics Provides Mechanistic Indicators of Mixture Toxicology for IMX-101 and IMX-104 Formulations in Fathead Minnows (*Pimephales promelas*). *Aquat. Toxicol.* **2018**, *199*, 138−151.

(14) Cassee, F. R.; Groten, J. P.; van Bladeren, P. J.; Feron, V. J. Toxicological Evaluation and Risk Assessment of Chemical Mixtures. *Crit. Rev. Toxicol.* **1998**, *28*, 73−101.

(15) Joanne, P.; Domingues, I.; Marta, M. Synergistic Effects Caused by Atrazine and Terbuthylazine on Chlorpyrifos Toxicity to Early-life Stages of the Zebrafish Danio rerio. *Environ. Sci. Pollut. Res.* **2000**, *20*, 4671−4680.

(16) Belden, J. B.; Lydy, M. J. Impact of Atrazine on Organophosphate Insecticide Toxicity. *Environ. Toxicol. Chem.* **2000**, *19*, 2266−2274.
(17) Panz, K.; Miksch, K.; Sójka, T. Synergetic Toxic Effect of An Explosive Material Mixture in Soil. *Bull. Environ. Contam. Toxicol.* **2013**, *91*, 555−559.
(18) Boyenle, I. D.; Divine, U. C.; Adeyemi, R.; Ayinde, K. S.; Olaoba, O. T.; Apu, C.; Adelusi, T. I.; et al. Direct Keap1-Kelch Inhibitors as Potential Drug Candidates for Oxidative Stress-Orchestrated Diseases: A Review on In silico Perspective. *Pharmacol. Res.* **2021**, *167*, No. 105577.
(19) Paloncýová, M.; Karel, B.; Michal, O. Molecular Insight into Affinities of Drugs and Their Metabolites to Lipid Bilayers. *J. Phys. Chem. B* **2013**, *117*, 2403−2410.
(20) Sujak, A. Interactions between Canthaxanthin and Lipid Membranes-Possible Mechanisms of Canthaxanthin Toxicity. *Cell. Mol. Biol. Lett.* **2009**, *14*, 395−410.
(21) Auluck, P. K.; Caraveo, G.; Lindquist, S. α-Synuclein: Membrane Interactions and Toxicity in Parkinson's Disease. *Annu. Rev. Cell Dev. Biol.* **2010**, *26*, 211−233.
(22) Yang, H.; Li, H.; Liu, L.; Zhou, Y.; Long, X. Molecular Simulation Studies on the Interactions of 2,4,6-Trinitrotoluene and Its Metabolites with Lipid Membranes. A Computational Study. *J. Phys. Chem. B* **2019**, *123*, 6481−6491.
(23) Yang, H.; Li, H.; Zhou, M.; Wei, T.; Tang, C.; Liu, L.; Zhou, Y.; Long, X. A Relationship between Membrane Permeation and Partitioning of Nitroaromatic Explosives and Their Functional Groups. A computational study. *Phys. Chem. Chem. Phys.* **2020**, *22*, 8791−8799.
(24) Jo, S.; Kim, T.; Iyer, V. G.; Im, W. CHARMM-GUI: A Web-based Graphical User Interface for CHARMM. *J. Comput. Chem.* **2008**, *29*, 1859−1865.
(25) Walsh, M. R.; Walsh, M. E.; Ramsey, C. A.; et al. Energetic Residues from the Detonation of IMX-104 Insensitive Munitions. *Propellants Explos. Pyrotech.* **2014**, *39*, 243−250.
(26) Van Der Spoel, D.; Lindahl, E.; Hess, B.; Groenhof, G.; Mark, A. E.; Berendsen, H. J. GROMACS: Fast, Flexible, and Free. *J. Comput. Chem.* **2005**, *26*, 1701−1718.
(27) Feller, S. E.; MacKerell, A. D. An Improved Empirical Potential Energy Function for Molecular Simulations of Phospholipids. *J. Phys. Chem. B* **2000**, *104*, 7510−7515.
(28) Jorgensen, W. L.; Chandrasekhar, J.; Madura, J. D.; Impey, R. W.; Klein, M. L. Comparison of Simple Potential Functions for Simulating Liquid Water. *J. Chem. Phys.* **1983**, *79*, 926−935.
(29) Hess, B. P-LINCS: A Parallel Linear Constraint Solver for Molecular Simulation. *J. Chem. Theory Comput.* **2008**, *4*, 116−122.
(30) Miyamoto, S.; Kollman, P. A. Settle: An Analytical Version of the SHAKE and RATTLE Algorithm for Rigid Water Models. *J. Comput. Chem.* **1992**, *13*, 952−962.
(31) Darden, T.; York, D.; Pedersen, L. Particle Mesh Ewald: An N·log (N) Method for Ewald Sums in Large Systems. *J. Chem. Phys.* **1993**, *98*, 10089−10092.
(32) Bussi, G.; Donadio, D.; Parrinello, M. Canonical Sampling Through Velocity Rescaling. *J. Chem. Phys.* **2007**, *126*, No. 014101.
(33) Parrinello, M.; Rahman, A. Polymorphic Transitions in Single Crystals: A New Molecular Dynamics Method. *J. Appl. Phys.* **1981**, *52*, 7182−7190.
(34) Vanommeslaeghe, K.; Hatcher, E.; Acharya, C.; Kundu, S.; Zhong, S.; Shim, J.; Mackerell, A. D., Jr.; et al. CHARMM General Force Field: A Force Field for Drug-like Molecules Compatible with the CHARMM All-Atom Additive Biological Force Fields. *J. Comput. Chem.* **2010**, *31*, 671−690.
(35) Mayne, C. G.; Saam, J.; Schulten, K.; Tajkhorshid, E.; Gumbart, J. C. Rapid Parameterization of Small Molecules Using the Force Field Toolkit. *J. Comput. Chem.* **2013**, *34*, 2757−2770.
(36) Meylan, W. M.; Howard, P. H.; Boethling, R. S.; Aronson, D.; Printup, H.; Gouchie, S. Improved Method for Estimating Bioconcentration/Bioaccumulation Factor from Octanol/water Partition Coefficient. *Environ. Toxicol. Chem.* **1999**, *18*, 664−672.
(37) Anézo, C.; de Vries, A. H.; Höltje, H. D.; Tieleman, D. P.; Marrink, S. J. Methodological Issues in Lipid Bilayer Simulations. *J. Phys. Chem. B* **2003**, *107*, 9424−9433.
(38) Tieleman, D. P.; Forrest, L. R.; Sansom, M. S.; Berendsen, H. J. Lipid Properties and the Orientation of Aromatic Residues in OmpF, Influenza M2, and Alamethicin Systems: Molecular Dynamics Simulations. *Biochemistry* **1998**, *37*, 17554−17561.
(39) Kumar, S.; Rosenberg, J. M.; Bouzida, D.; Swendsen, R. H.; Kollman, P. A. The Weighted Histogram Analysis Method for Free-Energy Calculations on Biomolecules. I. The Method. *J. Comput. Chem.* **1992**, *13*, 1011−1021.
(40) Hub, J. S.; De Groot, B. L.; Van Der Spoel, D. A free Weighted Histogram Analysis Implementation Including Robust Error and Autocorrelation Estimates. *J. Chem. Theory Comput.* **2010**, *6*, 3713−3720.
(41) Kulkarni, M.; Chaudhari, A. J. Microbial Remediation of Nitro-aromatic Compounds: an Overview. *J. Environ. Manage.* **2007**, *85*, 496−512.
(42) Marrink, S. J.; Berendsen, H. J. Simulation of Water Transport through a Lipid Membrane. *J. Phys. Chem. A* **1994**, *98*, 4155−4168.
(43) Qiao, R.; Roberts, A. P.; Mount, A. S.; Klaine, S. J.; Ke, P. C. Translocation of C60 and Its Derivatives across a Lipid Bilayer. *Nano Lett.* **2007**, *7*, 614−619.
(44) Riahi, S.; Rowley, C. N. Why Can Hydrogen Sulfide Permeate Cell Membranes? *J. Am. Chem. Soc.* **2014**, *136*, 15111−15113.
(45) Zeliger, H. I. Toxic Effects of Chemical Mixtures. *Arch. Environ. Health* **2003**, *58*, 23−29.
(46) Endo, S.; Escher, B. I.; Goss, K. U. Capacities of Membrane Lipids to Accumulate Neutral Organic Chemicals. *Environ. Sci. Technol.* **2011**, *45*, 5912−5921.
(47) Desai, P. V.; Raub, T. J.; Blanco, M. J. How Hydrogen Bonds Impact P-glycoprotein Transport and Permeability. *Bioorg. Med. Chem. Lett.* **2012**, *22*, 6540−6548.
(48) Alex, A.; Millan, D. S.; Perez, M.; Wakenhut, F.; Whitlock, G. A. Intramolecular Hydrogen Bonding to Improve Membrane Permeability and Absorption in Beyond Rule of Five Chemical Space. *Med. Chem. Commun.* **2011**, *2*, 669−674.
(49) Wang, H.; Meng, F. Concentration Effect of Cimetidine with POPC Bilayer: A Molecular Dynamics Simulation Study. *Mol. Simul.* **2016**, *42*, 1292−1297.
(50) Begnini, F.; Geschwindner, S.; Johansson, P.; Wissler, L.; Lewis, R. J.; Danelius, E.; Luttens, A.; Matricon, P.; Carlsson, J.; Lenders, S.; König, B.; Friedel, A.; Sjö, P.; Schiesser, S.; Kihlberg, J. Importance of Binding Site Hydration and Flexibility Revealed When Optimizing a Macrocyclic Inhibitor of the Keap1−Nrf2 Protein−Protein Interaction. *J. Med. Chem.* **2022**, *65*, 3473−3517.

https://doi.org/10.1021/acsomega.2c03886
ACS Omega 2022, 7, 40892−40899